ATTITUDE CONTROL OF A SPIN-STABILIZED NANO SATELLITE USING A SUN-POINTING ALGORITHM

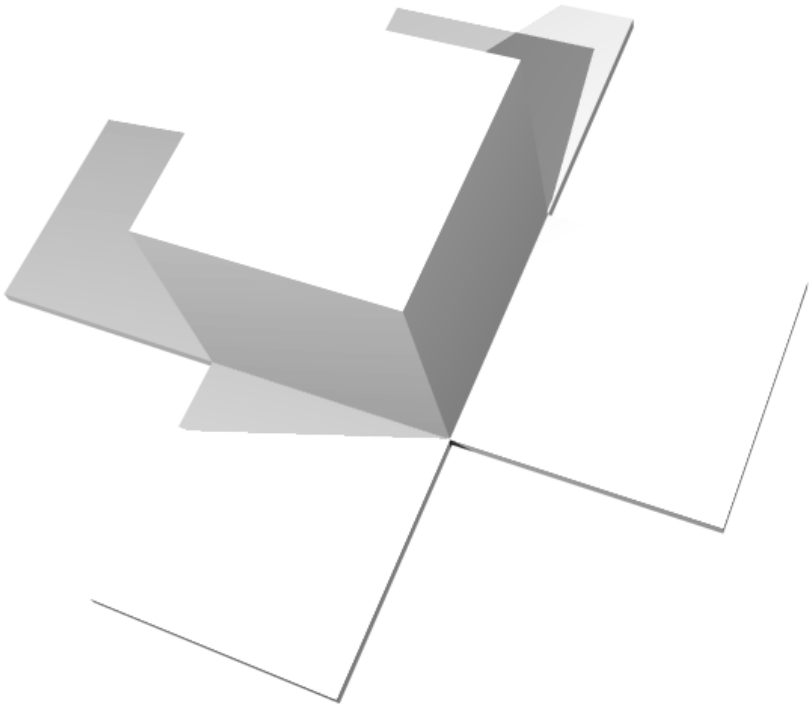

JOHAN SYLWANDER & DANIEL ÅBERG

KTH 2000
STOCKHOLM SWEDEN
TRITA 9110

ABSTRACT

In a collaboration between the Swedish Royal Institute of Technology (KTH), the IRF and the Swedish Space Corporation, a nano satellite is being developed under the name Victoria. The main objectives of the project are to test the implementation of attitude control using a Sun-pointing algorithm with a single electromagnetic coil as an actuator, and to take images of scientific interest. The following paper investigates the mentioned Sun-pointing algorithm and simulates its orbit behaviour in a Matlab-based space environment (the Spacecraft Control Toolbox). Numerous disturbance factors affecting the orbit of a satellite are discussed and several models of the Earth's magnetic field are used, in order to emulate space flight conditions as closely as possible. Ultimately, the power consumed by the attitude control algorithm was measured for different scenarios to facilitate comparing the efficiency with other control methods.

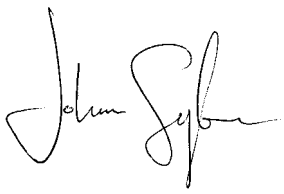

Johan Sylwander Daniel Åberg

Stockholm Sweden, December 2000

CONTENTS

1 INTRODUCTION

1.1 A BRIEF SATELLITE HISTORY

The idea of placing a satellite in space was first thought of by Sir Isaac Newton in 1687, at which time the actual process of launching and maintaining an object in orbit was an impossible task. In the year 1957 however, when rocket science and electronics had finally evolved sufficiently, Sputnik 1 was launched. It simply emitted a radio beep that could be recieved from Earth, but this was enough to qualify as an orbiting satellite. The next launch was made one month later, again by the Russians, as a dog named 'Laika' became the first living creature to leave Earth for space. The U.S. were quick to follow with a succesful launch of the satellite Explorer 1 in February 1958. Three years later, on April 12th 1961, the Russian Yuri A. Gagarin became the first man in space.

Then followed launches of several geostationary (rotating with the Earth and thereby giving the impression being stationary) tele-communications satellites before finally, on July 21st 1969, the first man (Neil Armstrong) walked the face of the moon. Today, the american space shuttle has the capabilities to bring back satellites from orbit for complicated repairs as well as sending people to and from either MIR or the International Space Station (ISS). During the last 50 years, satellites have evolved in terms of the technical aspect, fitting more complex systems into smaller areas, but they still contain the same basic components. These components include some sort of altitude meter, usually a radar on normal size satellites, solar panels and batteries. The panels collect energy while the battery stores the power for use while the satellite is in the shadow of the Earth. Some special cases also have employed nuclear power sources. The use of telemetry equipment allows for tracking of the satellite's systems from Earth via radio transmitters. Furthermore, attitude-control equipment such as thrusters, electromagnetic coils or actuator wheels is needed to point panels, sensors or antennae in desired directions.

1.2 NANO SATELLITES

Refined electronics and materials research has recently rendered it possible to build satellites weighing less than 10 kg. This creates possibilities for smaller nations, companies or even universities to become involved in space research or commercial ventures by launching their own small satellites. One benefit of designing and launching a nano satellite is the considerably shorter turn around time (time from conceptual idea to finished product), making it interesting for educational projects. In addition, a simplified system architecture with fewer onboard instruments facilitates coding of basic attitude control algorithms.

The concept of nano satellites poses some unique problems in the design phase of a new spacecraft. The main concern is that, because of the substantially lower mass, instabilities are easily introduced while adjusting the attitude of a spin stabilized nano satellite. To avoid increasing nutations (eventually leading to tumbling or flat spin) during attitude control, the rigid

body inertia matrix should emulate that of a flat, circular disc as closely as possible. Due to this problem, nano satellites have traditionally been equipped with unidirectional instruments, not making use of the full potential of a scientific satellite. Improved attitude control in nano satellites is therefore desirable in both scientific and commercial applications. For example, a number of small satellites could be combined into a formation orbiting array, giving increased capabilities, similar to combinations of small radio telescopes on the surface of Earth.

At present, the Munin satellite program [1], initiated by the Swedish Institute for Space Physics (IRF), the Universities of Umeå and Luleå as well as the Southwest Research Institute in the U.S., is aiming at launching a scientific nano satellite weighing 6 kg. The Munin satellite will employ a passive attitude control system using a permanent magnet, attempting to align the spacecraft with the magnetic field of the Earth. This simple attitude control mechanism should prove sufficient in pointing the satellite over the poles, where the planned experiments will take place. For Hugin [2] however, a satellite developed mainly by the Royal Institute of Technology (KTH), different ways of controlling the attitude will be implemented. In 1999, a project work entitled *'Attitude Control of a Nanosatellite using Reinforcement Learning Neural Networks'* [3] was published, dealing with the application of a neural network for attitude control purposes. In the following pages another satellite, named Victoria, will be used to evaluate an algorithm written by Sven Grahn of the Swedish Space Corporation (SSC). Its aim is to control the attitude of a spinning nano satellite by pointing the spin axis toward the Sun.

1.3 THE VICTORIA SATELLITE

The Victoria satellite project is the result of cooperation between the IRF, SSC and the Instrumentation group at the Physics Department of KTH. Primarily, the objectives of building the nano satellite are to evaluate magnetic attitude control and instrument applications. Previous work has been performed on the application of a neural network, which was taught to control the Hugin satellite's attitude either on the ground or in orbit. In the following project work, only one electromagnetic coil is used by the attitude control algorithm, instead of the three used in Hugin, reducing the power consumption substantially and simplifying the internal structure of the satellite. The launch location of the satellite is not yet determined, but it may take place at the Krunichev State Research and Production Space Center, with the satellite strapped onto a larger payload inside a 'Rockot' launch vehicle. The basic layout of Victoria is shown in Fig. (1.1) below, with dimensions and the spin axis marked.

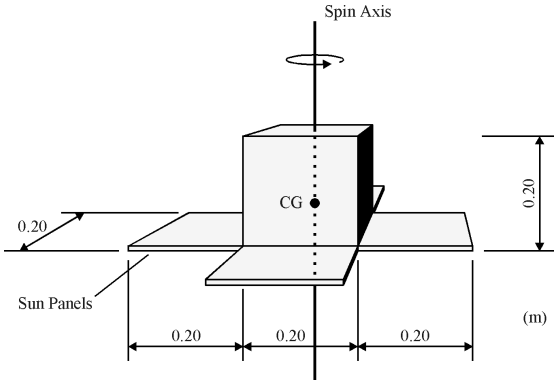

Figure 1.1. The solar panels are mounted 'facing down' on the horizontal plates.

Since the Victoria project is managed by a university, as opposed to a commercial firm, the financial resources available are somewhat limited. It is therefore necessary to minimize cost levels in the components and the manufacturing of the satellite, making the final product significantly less expensive than its commercial counterpart. One way to lower cost is to purchase off-the-shelf components, for example the camera is likely to be a standard webcam (QuickCam) with a modified casing to shield the electronics from radiation.

1.3.1 Subsystems

The satellite consists of several subsystems, interacting to achieve tasks such as attitude control or the taking of pictures. In the core of the miniturized network inside the spacecraft, the payload computer is located (see Fig. (1.2)). It is assigned to process data from the camera, Sun sensor and magnetometer as well as feed the torque coil with the correct current according to the attitude control algorithm. Furthermore, the payload computer, which is a standard Intel 9.8 MHz 8088 CPU, will communicate with the housekeeping computer. This computer oversees the sending or recieving of radio signals from ground control and the charging of the onboard batteries via the solar cells.

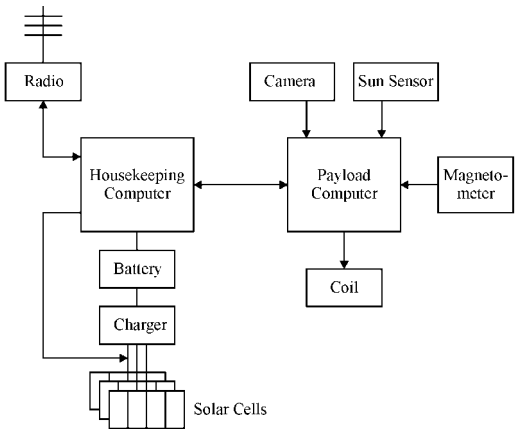

Figure 1.2. The satellite subsystems

During operation, the magnetometer constantly supplies the payload computer with angular velocity measurements needed in the determination of rotation and attitude. The Sun sensor has a field-of-view (FOV) of ± 20° and delivers the direction toward the Sun with high accuracy (errors << 1°). If need should ever arise to change the governing program in the payload computer, it can be done by sending the replacement code to the housekeeping computer, which then uploads it to the payload computer.

1.3.2 Mission Objectives

The satellite will be launched into a Sun-synchronous orbit (i.e. it newer enters the eclipse) at an altitude of 700 km above sea level and with a spin rate of 10 rpm. A Sun-synchronous orbit is achieved using the fact that the Earth's slight bulge at the equator acts to slowly rotate the plane of the orbit about the axis of the Earth. When the inclination is chosen just right (about 8° off the polar orbit) the motion matches the motion of the Sun across the sky. Thus, the plane of the orbit executes one full rotation about the axis of the Earth in one year.

In orbit, the spacecraft will attempt to align the spin axis with the Sun vector in an antiparallel fashion, directing the solar panels toward the Sun. The function of the camera is limited as a result of the constant spin rate, but it will used as efficiently as possible. Optimal radio reception is obtained when the antenna is directed tangentially to the Earth's surface at the ground control fly-by. A suitable placement of antennae might therefore be on the location of the spin axis.

1.3.3 Attitude Control

The attitude control will be managed by an algorithm based on the paper *'An On-board Algorithm for Automatic Sun-pointing of a Spinning Satellite'* [4] by Sven Grahn. It utilizes one electromagnetic coil placed in the plane orthogonal to the spin axis of Victoria to generate a dipole moment which in reciprocal action with the Earth's magnetic field exerts a torque on the satellite. By switching the current direction (polarity) of the coil, the torque can be selected to 'guide' the spin axis toward the half-plane containing the projected direction of the Sun, as shown in Fig. (1.3). This algorithm has the distinct advantage of simplicity; it only requires a few computations at each time step in the payload computer. The power consumption of the single coil turns out to be quite low, especially when the satellite has settled on a desired attitude. In that scenario, the algorithm sends short bursts of current through the coil to counteract any increases in oscillation of the spin axis.

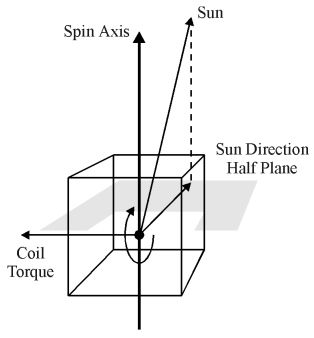

Figure 1.3. Orientation of the torque

2 THEORY

2.1 ORBITAL MECHANICS

Below, derivations of the most common governing equations in orbital dynamics are presented. The number of steps in each deduction has been kept to a minimum in order to promote reading comprehension.

2.1.1 The Two-Body Central Force Problem

Consider two particles with masses m_1 and m_2 and position vectors $\mathbf{r}_1$ and $\mathbf{r}_2$ respectively (Fig. (2.1)). Assume that the only forces affecting the particles are the forces with which they act upon each other: $\mathbf{F}_{21}$ from particle number 2 on number 1, and $\mathbf{F}_{12}$ from 1 on 2. The equations of motion are then

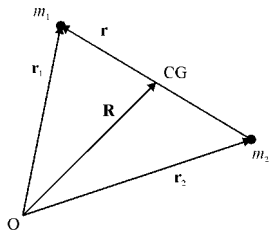

Figure 2.1. Two-body motion

$$m_1\ddot{\mathbf{r}}_1 = \mathbf{F}_{21} \tag{2.1}$$
$$m_2\ddot{\mathbf{r}}_2 = \mathbf{F}_{12} \tag{2.2}$$

According to Newton's third law, $\mathbf{F}_{21}$ is equal to - $\mathbf{F}_{12}$ so the two equations of motion can be added together, giving:

$$m_1\ddot{\mathbf{r}}_1 + m_2\ddot{\mathbf{r}}_2 = \mathbf{0} \tag{2.3}$$

With the help of the center of mass vector $\mathbf{R} = (m_1\mathbf{r}_1 + m_2\mathbf{r}_2)/(m_1 + m_2)$ and the notation $M = m_1 + m_2$ this yields the following

$$M\ddot{\mathbf{R}} = \mathbf{0} \tag{2.4}$$

Eq. (2.4) shows that there is no force on the center of mass. Hence, the center of mass remains at rest or moves with constant velocity depending on the inertial reference frame. Since the sum of the equations produced something interesting in Eq. (2.3), maybe the difference should be examined as well. By first dividing Eq. (2.1) with m_1 and Eq. (2.2) with m_2 and then subtracting the resulting equation for particle 2 from that of particle 1 this is obtained:

$$\left(\ddot{\mathbf{r}}_1 - \ddot{\mathbf{r}}_2\right) = \left(\frac{1}{m_1} + \frac{1}{m_2}\right)\mathbf{F}_{21} \tag{2.5}$$

If $\mathbf{r} = \mathbf{r}_1 - \mathbf{r}_2$ and $\mu = (1/m_1 + 1/m_2)^{-1} = m_1m_2/(m_1 + m_2)$, it can be rewritten as

$$\mu\ddot{\mathbf{r}} = \mathbf{F}_{21} \tag{2.6}$$

This demonstrates that the position vector of particle 1 relative to particle 2 obeys an equation of motion in which the so-called *reduced mass* μ plays the role of (inertial) mass and the force is the force on particle 1 from particle 2.

Thus, one can formally treat the two particle problem as a one particle problem, where the mass is the reduced mass.

2.1.2 Energy Conservation for a Central Force

The magnitude of a central force will only depend on the distance from the center: $\mathbf{F}(\mathbf{r}) = F_r(r)\mathbf{e}_r$, which means that the force is conservative and the potential energy can be written as

$$\Phi(r) = -\int_r F_r(r)\mathrm{d}r \tag{2.7}$$

Since the motion is confined to a plane (the [*x*, *y*] - plane) it seems suitable to use cylindrical coordinates, specifying the position with the radius ρ and angle φ. The law of conservation of energy, using cylindrical coordinates, states

$$\frac{1}{2}mv^2 + \Phi(\rho) = \frac{1}{2}m\left(\dot{\rho}^2 + \rho^2\dot{\varphi}^2\right) + \Phi(\rho) = E \tag{2.8}$$

where *m* is the mass, *v* the velocity and *E* is the total energy.

Recalling a basic law of dynamics, it is necessary that the angular momentum $L = m\rho^2\varphi$ is constant since the motion is confined to a plane and the central force field gives zero torque. Hence, the energy equation can be rewritten in terms of ρ and its time-derivative as follows

$$\frac{1}{2}m\left(\dot{\rho}^2 + \frac{L^2}{m^2\rho^2}\right) + \Phi(\rho) = E \tag{2.9}$$

If an *effective potential* energy function Φ_{eff} is introduced on the form

$$\Phi_{eff}(\rho) = \frac{L^2}{2m\rho^2} + \Phi(\rho) \tag{2.10}$$

then the energy conservation in terms of the radial motion will look like a one-dimensional energy conservation:

$$\frac{1}{2}m\dot{\rho}^2 + \Phi_{eff}(\rho) = E \tag{2.11}$$

Now assume that the force is of the form (given by Newton's universal law of gravitation)

$$F_\rho(\rho) = -\frac{K}{\rho^2} \tag{2.12}$$

where $K = Gm_1m_2$ in the case of gravity. Consequently, the potential energy $\Phi(\rho)$ can be stated as

$$\Phi(\rho) = -\frac{K}{\rho} \tag{2.13}$$

making the effective potential energy function look like this:

$$\Phi_{eff}(\rho) = \frac{L^2}{2m\rho^2} - \frac{K}{\rho} \tag{2.14}$$

One useful application of this equation is to find the *turning-points* in the radial motion. These correspond to the maximum and minimum values of ρ, hence the first time derivative of ρ is zero or there is no radial velocity. Thus, Eq. (2.11) gives the following expression for the ρ-values of these turning-points:

$$\frac{L^2}{2m\rho^2} - \frac{K}{\rho} = E \tag{2.15}$$

This quadratic equation is easily solved and the roots are given by

$$\frac{1}{\rho_{\pm}} = \frac{mK}{L^2} \pm \sqrt{\left(\frac{mK}{L^2}\right)^2 + \frac{2mE}{L^2}} \tag{2.16}$$

Note that the energy E may be negative here (E gives the shape of the trajectory). However, the smallest physically allowed value of the energy is that which makes the expression under the square root zero:

$$E_{\min} = -\left(\frac{mK}{L^2}\right)^2 \frac{L^2}{2m} = -\frac{mK^2}{2L^2} \tag{2.17}$$

For this minimum energy the ρ-value of the trajectory must be given by the constant $\rho = L^2/(mK)$ and the trajectory is thus a circle with this radius. If the energy E is positive, one root becomes negative and must be discarded, hence the radial motion has only one minimum ρ-value and the trajectory extends to infinity. This type of motion is called unbound. When the motion lies between two turning-points, it is called bound and this can only happen when the energy is negative $E < 0$, since $K = Gm_1m_2$ is always positive.

2.1.3 The Kepler Problem

In the previous section it was shown that the problem of the radial motion, in the inverse square central force field, $F_\rho = -K/\rho^2$, can be solved using conservation of energy and angular momentum. Physically that model describes the motion of a moon around a planet. Now an attempt to solve for the angular motion will be made. The equations of motion in terms of cylindrical coordinates are:

$$m\left(\ddot{\rho} - \rho\dot{\varphi}^2\right) = F_\rho \tag{2.18}$$

$$m\left(\rho\ddot{\varphi} + 2\dot{\rho}\dot{\varphi}\right) = 0 \tag{2.19}$$

The preferred form for the solutions of these equations would be on the parametric form $(\rho(t), \varphi(t))$. Unfortunately, solving that problem is quite difficult and so the best approach would be to solve the equations numerically. However, it turns out that if the time t is eliminated and only the shape of the trajectory as a relationship between ρ and φ is seeked, for instance on the form $\rho = f(\varphi)$, the problem can be treated analytically. This is often referred to as the *Kepler problem* since it was Johannes Kepler who empirically found the shape of the planetary trajectories. The analytical solution to this problem is (for a step-by-step solution see [5]):

$$\rho = \frac{p}{1 + e\cos\varphi} \tag{2.20}$$

where $p = \frac{L^2}{mK}$ and $e = Ap = \pi a^2 p$ in the case of a circular orbit.

Eq. (2.20) constitutes the desired relationship between ρ and φ, which gives the shape of the trajectory. The shape is a so-called 'conic section' (quadratic curve) and these are defined in Tab. (2.1) below, for different values of the eccentricity e.

$e = 0$	circle
$0 < e < 1$	ellipse
$e = 1$	parabola
$e > 1$	hyperbola

Table 2.1. The eccentricity determines the shape of the trajectory.

2.1.4 Kepler's Laws

The German astronomer Johannes Kepler (1571-1630) established three physical laws that predicted the motions of the planets around the Sun. These laws also govern a satellite's orbit around the Earth. Kepler stated that:

1. Every planet moves in an orbit that is an ellipse, with the Sun at one focus of the ellipse.
2. The radius vector drawn from the Sun to any planet sweeps out equal areas in equal time.
3. The squares of the periods of revolution of the planets are proportional to the cubes of the semimajor axes of their orbits.

The first law defines the geometry of the orbit, whereas the second law determines the velocity of the satellite along the orbit. Finally, the third law predicts the time of a revolution around the Earth.

Later on Sir Isaac Newton (1642-1727) established the three laws of motion and, from them, the universal law of gravitation. Newton's theory of gravitation produced a theoretical principle that explained the motions of the planets and laid the foundation for modern space flight. The law of gravitation as well as the conservation of mechanical energy and angular

momentum yields the equations of motion for any satellite orbit around the Earth. These equations are described mathematically by three scalar second-order differential equations. The integration of these equations of motion produces six constants of integration. These constants of integration are known as the orbital elements. The Keplarian orbital elements are often referred to as classical or conventional elements and are the easiest to use.

2.1.5 The Keplarian Orbital Elements

This set of orbital elements can be divided into two groups: the dimensional elements and the orientation elements. Both groups can be seen in Fig. (2.2) below:

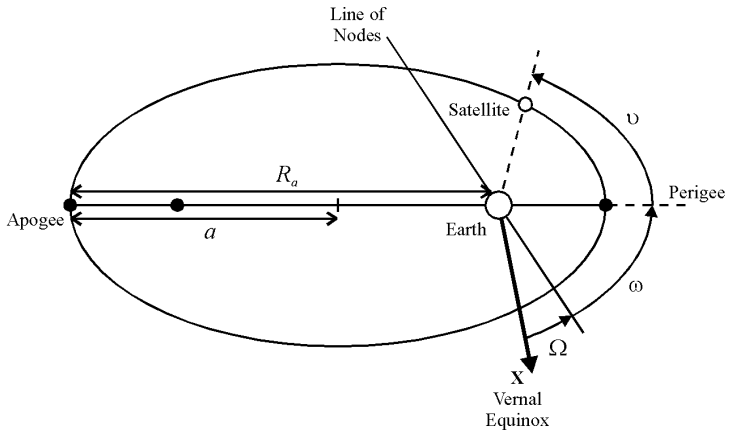

Figure 2.2. The Earth and the middle black dot constitute the focal points of the ellipse.

The dimensional elements specify the size and shape of the orbit and relate the position in the orbit to time. They are defined as follows:

1. The semimajor axis of the ellipse (a), which specifies the size of the orbit.
2. The eccentricity (e), which specifies the shape of the orbit ($e = 0$ results in a circular orbit).
3. The true anomaly (υ) giving the satellite position at any given time along the orbit. The true anomaly is the angle between the perigee and the position vector of the satellite.

The orientation elements specify the orientation of the orbit in space. They are defined as follows:

4. The inclination (i) of the orbit plane (shown in Fig. (2.3)) with respect to the reference plane, which is taken to be the Earth's equator plane for satellite orbits.
5. The right ascension of the ascending node (Ω), which is the angle between the ECI (described below) systems x-axis (in the direction of the Vernal Equinox) to the point at which the satellite makes its south-to-north crossing of the equator (ascending node). This element gives the orientation of the

orbit plane relative to the x-axis of the ECI coordinate system.

6. The argument of perigee (ω), measured in the orbit plane in the direction of motion, from the ascending node to perigee. The angle ω then specifies the orientation of the orbit in its plane.

These six orbital elements (a, e, υ, i, Ω, ω) define the satellite's position in space at any given time. Furthermore, the *Apogee* is the longest distance a vehicle gets from the Earth in its orbit and the *Perigee* is the closest it comes in orbit. R_a defines the distance from the center of the Earth to the apogee and the *Line of Nodes* is the point where the satellite crosses the Equator.

2.1.6 The ECI System

Several coordinate systems are used in the study of the motions of the Earth and other celestial bodies. However, the geocentric-equatorial coordinate system is the most suitable one when studying the motion of satellites around the Earth. This system has its origin at the Earth's center with the Z-axis pointing in the direction of the North Pole. The positive X-axis points in the direction of the Vernal Equinox. This direction is a line joining the center of the Earth with the center of the Sun at the first day of spring (all Earth locations experience identical durations of daylight and darkness). This direction is sometimes denoted by the head of a ram's head (♈) by astronomers because it points in the direction of the constellation Aries. The Y-axis completes the right-handed coordinate system. It is important to keep in mind that this coordinate system is not fixed to the Earth nor turning with it; the Earth turns relative to it. The Earth's spin axis wobbles slightly and shifts in direction slowly over centuries, an effect known as precession. As a result, where extreme precision is required, it is necessary to specify the coordinates of an object based on a particular year or epoch.

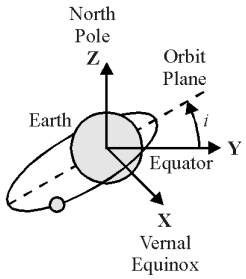

Figure 2.3. The ECI System

2.2 ORBIT PERTURBATIONS

By definition, small deviations from a two-body orbit motion are called orbit perturbations. The two-body orbit motion (e.g. a spacecraft orbiting a planet) can result in one of the conic solutions (ellipse, hyperbola and parabola) in closed form. Deriving the equations of two-body motion and their solutions can be done through Newton's law of gravitation and Kepler's laws of orbit motion under the assumption of point mass or mass with spherically symmetrical distribution. However, the accuracy of this model decreases as the time of propagation increases. Perturbing forces include Earth gravity harmonics (deviations from a perfect sphere), the lunisolar gravitational attractions, atmospheric drag, solar radiation pressure and Earth tides. The magnitude of all the perturbing accelerations is at least one order of magnitude less than the two-body acceleration, hence the term 'perturbations'.

2.2.1 Earth Gravity Harmonics

The gravity field of a body with finite mass can be represented by a potential function. If the mass of a celestial body is assumed to be a point mass or uniformly distributed in a sphere, the potential function takes the following simple form:

$$\Phi = \frac{\mu}{r} \tag{2.21}$$

Eq. (2.21) indicates that the strength of the gravity potential at a point in space is directly proportional to the mass of the body ($\mu = GM$, where G is the gravitational constant and M is the mass) and inversely proportional to the distance r to the center of the body. From potential theory, the gravitational force or acceleration along a given direction is equal to the partial derivative or gradient of the potential in that direction. In reality, the point-mass potential cannot accurately represent the gravity field of the Earth and other planets in the solar system because of the nonspherical shape of these bodies. Instead, the potential function should be derived from a spheroid that can closely represent the shape and mass distribution of the Earth or other planets. The development of the potential of a spheroid requires an extensive mathematical integration over the entire body, for a complete description of this potential function see [6].

$$\Phi = \frac{\mu}{r}\left[1 - \sum_{n=2}^{\infty}\left(\frac{a_e}{r}\right)^n J_n P_n(w)\right] \tag{2.22}$$

Here a_e is the equatorial radius of the body, P_n are so-called Legendre polynomials, w is the declination of the satellite and the J_n coefficients are described below. This new potential function results in a phenomenon referred to as *gravity harmonics*. There are three sets of harmonics: the *zonal harmonics, sectorial harmonics* and *tesseral harmonics*. They constitute the terms of a mathematical expansion through which the deviations from a sphere can be represented. The most commonly encountered gravity harmonics are J_2 and J_{22}, which are the largest terms of the zonal and tesseral harmonics. The coefficient of the second harmonic J_2 is related to the Earth equatorial oblateness through Earth rotation (the difference between the polar radius and equatorial radius). The J_2 coefficient is the source of the secular rates for the right ascension of ascending node, the argument of perigee, and a small correction to the mean motion of the orbit. The tesseral harmonic J_{22} is related to the ellipticity of the Earth equatorial plane and is responsible for the long-term (860 days) resonance effects on geosynchronous orbits. This harmonic causes geosynchronous satellites to drift from their longitude position, which must be controlled by periodic stationkeeping maneuvers.

2.2.2 Radiation Pressure Effects

Orbit perturbations induced by solar radiation are a result of photon momentum or radiation pressure on a space vehicle. At one astronomical unit (A.U.), the solar radiation pressure constant P_0 is $4 \cdot 10^{-10}$ N/cm^2. This

value may fluctuate slightly (by less than 1%) as a result of variations in the solar activity index. A typical radiation pressure effect on satellite orbits is the long-term sinusoidal variations in eccentricity. The magnitude of the variation is proportional to the effective area (the projected area of the satellite), surface reflectivity, and the inverse of the satellite mass. For a typical communication satellite in geosynchronous orbit, the eccentricity may vary from 0.001 to 0.004 in six months as a result of solar radiation pressure effects. For low-altitude orbits, the period of the long-term variation in eccentricity is governed by the combined rates of the longitude of the mean Sun, nodal regress and argument of perigee (described in [6]). Radiation pressure induces periodic variations in all orbital elements, even exceeding the effects of atmospheric drag at altitudes above 900 km.

2.2.3 Atmospheric Drag

When the orbit perigee height is below 1000 km, the atmospheric drag effect becomes increasingly important. Drag, unlike other perturbation forces, is a non-conservative force and will continuously take energy away from the orbit. Since the drag is greatest at perigee, where the velocity and atmospheric density are highest, the energy drain is also greatest at this point. Because of this energy decline, the elliptic orbit first becomes circular as the altitude of the apogee decreases to the same value as the perigee and then rapidly spirals into the dense atmosphere. For near circular orbits, the orbit semi-major axis decay rate can be computed by the following simple equation:

$$\frac{\mathrm{d}a}{\mathrm{d}t} = -na^2\left(\frac{\rho g_0}{B}\right) \tag{2.23}$$

where n is the mean motion (defined as the square root of μ/a^3), ρ is the atmospheric density at present altitude, g_0 is the gravitational acceleration at sea level and B is the ballistic coefficient (expresses a bullet's length and aerodynamic shape, thus indicating its ability to overcome air resistance in flight).

2.2.4 Lunisolar Gravitational Attractions

To understand the long-term behaviour of a satellite orbit under the influence of the Sun, imagine both the satellite and the Sun spread out into elliptical rings coinciding with their respective orbits, see Fig. (2.4). The mutual gravitational attractions of the rings will create a torque about the line of nodes tending to turn the satellite ring into the ecliptic. The gyroscopic effect of the torque on the spinning satellite ring will induce a gyro precession of the orbit about the pole of the ecliptic, specifically a regression of the nodes along the ecliptic. Similarly, the Moon will cause a regression of the orbit about an axis normal to the Moon's orbit plane, which has a 5° inclination with respect to the ecliptic plane with a node rate of one rotation in 18.6 years. For orbits with periods equal to 12 h or longer, the lunisolar effects are significant and should be included but for low-altitude orbits, the Sun-Moon effects can be neglected.

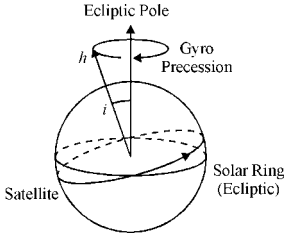

Figure 2.4. Gyroscopic precession

2.3 SPACECRAFT DYNAMICS

A basic account of the equations governing spacecraft dynamics is given in the following sections.

2.3.1 Euler's Equations of Motion

In spacecraft dynamics there is one fundamental equation that constitutes the foundation upon which many other expressions for rigid bodies are based. It can be formulated as follows: The angular momentum **L** of a rigid body, with one point fixed about the instantaneous axis of rotation through the fixed point, is defined by

$$\mathbf{L} = \sum_i m_i \left(\mathbf{r}_i \times \mathbf{v}_i\right) = \sum_i m_i \left(\mathbf{r}_i \times \left(\boldsymbol{\omega} \times \mathbf{r}_i\right)\right) \tag{2.24}$$

where m_i is the mass of the i^{th} particle, $\mathbf{r}_i$ is the vector pointing at particle P, $\boldsymbol{\omega}$ is the angular velocity about the instantaneous axis and the summation is performed over all particles in the body, see Fig. (2.5). If a fixed cartesian coordinate system is chosen, the components of the angular momentum can be written in this form:

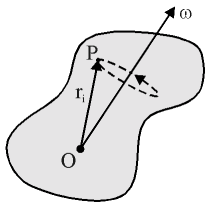

Figure 2.5. Rigid body rotation

$$\begin{cases} L_x = I_{xx}\omega_x + I_{xy}\omega_y + I_{xz}\omega_z \\ L_y = I_{yx}\omega_x + I_{yy}\omega_y + I_{yz}\omega_z \\ L_z = I_{zx}\omega_x + I_{zy}\omega_y + I_{zz}\omega_z \end{cases} \tag{2.25}$$

where, with $[x_i\ y_i\ z_i]$ being the cartesian coordinates to particle i,

$$\begin{aligned} &I_{xx} = \sum_i m_i \left(y_i^2 + z_i^2\right), \quad I_{yy} = \sum_i m_i \left(z_i^2 + x_i^2\right), \quad I_{zz} = \sum_i m_i \left(x_i^2 + y_i^2\right) \\ &I_{xy} = -\sum_i m_i x_i y_i = I_{yx}, \quad \ldots \end{aligned} \tag{2.26}$$

The quantities I_{xx}, I_{yy}, I_{zz} are called the *moments of inertia* about the x, y, and z axes respectively and the quantities I_{xy}, I_{xz} … are refered to as the *products of inertia*. For rigid bodies with a continuous mass distribution, these can be determined by integration over the body. From the I_{jk} elements, a symmetric matrix called the *inertia matrix* or *tensor* can be assembled:

$$\mathbf{I} = \begin{bmatrix} I_{xx} & I_{xy} & I_{xz} \\ I_{yx} & I_{yy} & I_{yz} \\ I_{zx} & I_{zy} & I_{zz} \end{bmatrix} \tag{2.27}$$

Developing the theory further, a special case of axes gives simplified calculations for rotating rigid bodies (extracted from [7]): *'A set of 3 mutually perpendicular axes having origin O which are fixed in the body and rotating with it and which are such that the products of inertia about them are zero, are called principal axes of inertia or briefly principal axes'*. For a body rotating around one of its principal axes, the direction of the

angular momentum is the same as that of the angular velocity, see Eq. (2.28):

$$\mathbf{L} = I\boldsymbol{\omega} \tag{2.28}$$

where I has a scalar value. This results in the following three equations (proof omitted here):

$$\begin{cases} (I_{xx} - I)\omega_x + I_{xy}\omega_y + I_{xz}\omega_z = 0 \\ I_{yx}\omega_x + (I_{yy} - I)\omega_y + I_{yz}\omega_z = 0 \\ I_{zx}\omega_x + I_{zy}\omega_y + (I_{zz} - I)\omega_z = 0 \end{cases} \tag{2.29}$$

For Eq. (2.29) to have non-trivial solutions, it is required that

$$\begin{vmatrix} I_{xx} - I & I_{xy} & I_{xz} \\ I_{yx} & I_{yy} - I & I_{yz} \\ I_{zx} & I_{zy} & I_{zz} - I \end{vmatrix} = \mathbf{0} \tag{2.30}$$

Solving the determinant yields three real-valued roots I_1, I_2 and I_3, called the *principal moments of inertia*. Computing the directions of the principal axes can be done by inserting the value of I_1, I_2 or I_3 into Eq. (2.29) which gives the relative magnitudes of ω_x, ω_y and ω_z and thereby the axis direction for the chosen principal moment of inertia. An axis of symmetry of a rigid body, such as the spin axis of Victoria, is always a principal axis. Since the inertial products are equal to 0 for rotations around principal axes, only the diagonal terms of Eq. (2.27) are non-zero for a symmetric spinning satellite (as long as the rotational axis is constant).

According to fundamental dynamics, the derivative of the angular momentum of a rigid body is equal to the total torque acting on the body. Differentiating the expression for **L** from Eq. (2.24), an important relation between the change in angular momentum and the torque **T** exerted on a rigid body is obtained:

$$\frac{d\mathbf{L}}{dt} = \sum_i \frac{d}{dt}(\mathbf{r}_i \times m_i \mathbf{v}_i) = \sum_i (\mathbf{r}_i \times \mathbf{F}_i) = \mathbf{T} \tag{2.31}$$

Moving to the spinning body frame one additional term is added:

$$\left(\frac{d\mathbf{L}}{dt}\right)_{space} = \left(\frac{d\mathbf{L}}{dt}\right)_{body} + \boldsymbol{\omega} \times \mathbf{L} = \mathbf{T} \tag{2.32}$$

The components of Eq. (2.32) can be calculated using the principal axes frame, arriving at

$$\begin{cases} T_1 = I_1\dot{\omega}_1 + (I_3 - I_2)\omega_2\omega_3 \\ T_2 = I_2\dot{\omega}_2 + (I_1 - I_3)\omega_3\omega_1 \\ T_3 = I_3\dot{\omega}_3 + (I_2 - I_1)\omega_1\omega_2 \end{cases} \tag{2.33}$$

These equations are known as *Euler's equations of motion* and are extremely useful in the study of rigid-body motion. The indices 1, 2 and 3 can be exchanged with the cartesian coordinates *x*, *y*, and *z* as long as these reference axes coincide with the principal axes of inertia and the origin is located at the center of gravity.

2.3.2 Magnetic Torque Coils

When a current is sent through a loop of wire, known as a coil, a dipole moment **m** is formed with a directional normal **n** given by the direction of the current in the coil, see Fig. (2.6). The moment is a product of the number of turns *N* in the coil, the applied current *I*, the cross-sectional area *A* of the coil (the area enclosed by one loop of wire) and the mentioned normal:

$$\mathbf{m} = NIA\hat{\mathbf{n}} \tag{2.34}$$

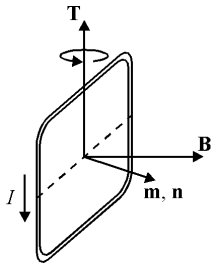

Figure 2.6. The torque on one loop of the electromagnetic coil

For the coil to exert a torque on the satellite and thereby control its attitude, some sort of reciprocal action with the surrounding environment is needed. Fortunately, a magnetic dipole that is exposed to an external magnetic field, such as the Earth's magnetic field shown in Fig. (2.7), will experience a torque. This torque **T** is given by the cross-product (from [8])

$$\mathbf{T} = \mathbf{m} \times \mathbf{B} \tag{2.35}$$

where **B** is the field vector of the Earth's magnetic field. Thus, by alternating the current in the coil and thereby changing the orientation of the dipole, the satellite's attitude can be adjusted.

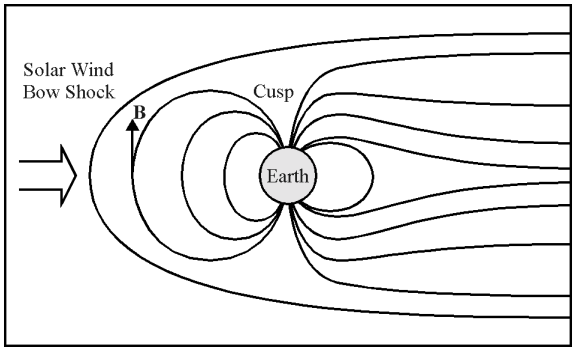

Figure 2.7. The Earth's magnetic field shape due to the solar wind (particle stream from the Sun)

2.4 SATELLITE DYNAMICS DUE TO DISTURBANCES

There are a number of disturbances (with numerous sources) acting on a satellite in orbit, introducing torques with different orientations that may cause the spacecraft to drift off course attitude-wise. Below, a brief account of the most common disturbance sources and their resulting torques is given.

2.4.1 Solar Radiation Pressure

Every surface that is illuminated by the Sun is exposed to solar emissions. These emissions consist mainly of photons, a particle which has a certain amount of energy that can be translated into mass and movement by employing Einstein's well known formula $E = mc^2$. Thus, when objects in space are hit by photons a pressure is exerted, giving a force directed away from the Sun. The phenomena was first detected nearly 400 years ago by the astronomer Johannes Kepler, who observed the way comets' tails always point away from the Sun. Light generated forces must not be confused with the solar wind, an extremely thin flow of particles ejected by the sun which exerts very little force on anything it hits. Torques due to solar radiation do not reach higher magnitudes than $8 \cdot 10^{-10}$, and will not be considered in the simulations.

2.4.2 Thermal Imbalances

To precisely determine the orbit, accelerations arising from the thermal gradients (temperature differences) across the spacecraft surfaces must be calculated. The level of infrared radiation that is emitted by a surface is proportional to the emissive properties of the material and to the fourth power of its temperature. The surface temperature varies with exposure to both external (i.e. solar radiation) and internal heat sources (i.e. electronics). Spacecraft often use both passive and active thermal control systems to regulate the temperature of electronic components. This may result in heat directionally expelled from the body, causing an acceleration. Modeling a satellite's overall thermal behaviour would require knowledge of the history of every surface's temperature and current exposure to heat sources, making the calculation rather tedious. Fortunately, thermal forces on the Victoria satellite measure in the range of $< 10^{-8}$ Newtons, and can therefore be disregarded in basic simulations.

2.4.3 Gravity Gradient

The gravity gradient disturbance torque appears due to any off-diagonal terms in the inertia matrix (shown in Eq. (2.27)). This gradient refers to the difference in the acceleration of gravity as the distance to Earth increases. For the orbit of a rigid body, the center of gravity follows the path of the orbit plane. Any points on the body that follow the path but are further from or closer to the Earth will cause a torque to be exerted around the center of gravity, because of the slightly different gravitational pull at each point. The torque vector is expressed as:

$$\mathbf{T}_{GG} = 3\omega_0^2 \begin{bmatrix} -I_{yz} \\ I_{xz} \\ 0 \end{bmatrix} \tag{2.36}$$

where ω_0 is a suitable rate of rotation. The contribution of $\mathbf{T}_{gg}$ to the rotational dynamics for a large satellite with long solar arrays warped by thermal distortion can be substantial. However, for a satellite of Victoria's

moderate size, with negligible inertial products (I_{xy}, I_{yx}, I_{yz}, …), the gravity gradient torque will not affect basic attitude control simulations.

2.4.4 Transmit Antennas Radiation Pressure

The majority of satellites today are equipped with antennas, transmitting signals with a certain power P. The contents of these transmissions may include Telecom, GPS, TV or steering commands. Due to the output power of the directional antenna, a torque (defined by Eq. (2.37)) will be produced around the spacecraft's center of gravity:

$$\mathbf{T}_{RF} = -\frac{P}{c}\mathbf{r}\times\mathbf{u} \tag{2.37}$$

where c is the speed of light ($3\cdot10^8$ m/s), **r** is the vector to the antenna boresight (the physical axis of a directional antenna) from the spacecraft center of gravity and **u** points in the direction opposite the antenna boresight, see Fig. (2.8). Internal radio frequency transmissions do not produce a net torque on the satellite. For high power satellites with offset reflectors, the torque can reach sufficiently high values to pose a problem. For example, a transmitting antenna with an output of 600 watts offset 3 m from the CG will generate a 6 μNm torque. Victoria's transmitter unit, with its 5 watt power consumption, can at most create a torque of ≈ 0.0033 μNm and will therefore be considered = 0 during calculations.

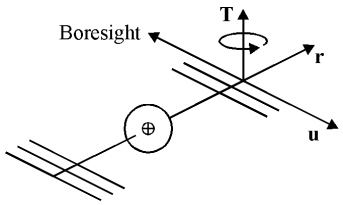

Figure 2.8. The RF Torque

2.4.5 Residual Dipoles

The phenomena of residual dipole disturbances comes from the interaction between the magnetic fields generated by internal current loops on the spacecraft and solar arrays with the Earth's magnetic field. In calculating these disturbances, the solar arrays and core of the satellite must be accounted for separately. The torque due to residual dipoles (for a generic two-panel satellite) is:

$$\mathbf{T}_{RD} = \left(\mathbf{M}_C + \mathbf{C}_N\mathbf{M}_N + \mathbf{C}_S\mathbf{M}_S\right)\times\mathbf{B} \tag{2.38}$$

where **B** is the Earth's magnetic field measured in the body frame, $\mathbf{C}_N$ is the transformation matrix that transforms from the north panel frame to the core frame, $\mathbf{C}_S$ is the south transformation matrix and $\mathbf{M}_i$ is the dipole for the i^{th} body. Typically each of the panels produce a dipole in the neighbourhood of 5 ATM^2 while the Earth's magnetic field magnitude is about 0.90 nT, giving each array a torque contribution of 0.45 μNm.

Two additional sources of disturbances worth mentioning are: leaks from onboard gas and liquid supplies and 'outgassing' of moisture embedded in the structure. Neither of these will be considered in the computer simulations.

2.5 SUN-POINTING ALGORITHM FOR A SPINNING SATELLITE

The attitude control algorithm used for Victoria is written by Sven Grahn of the Swedish Space Corporation and is applicable to any spin-stabilized satellite equipped with a Sun sensor, a magnetometer and an electromagnet. The aim of the algorithm is to point the spin axis, and thereby the solar panels located on the negative z-side of the satellite (see Fig. (1.1)), toward the Sun as accurately and continuously as possible for the purpose of recharging the onboard batteries. Previous Sun-pointing algorithms have usually incorporated a two-stage process in which the spin axis orientation in the Earth Centered Inertial (ECI) frame is calculated after which an appropriate current through the actuator coil(s) is computed by comparison to the Earth's magnetic field. Grahn's method however, requires neither the spin axis orientation nor the Sun vector in ECI coordinates. It is based on the following rule for the direction of current through a coil aligned with the spin axis: *'The direction of the current through the electromagnet shall be such that the magnetic dipole moment of the electromagnet along the spin axis has the same sign as the component of the Earth's magnetic field along an axis perpendicular to the plane defined by the spin axis and the direction toward the Sun'*. Fig. (2.9) below demonstrates the basic quantities:

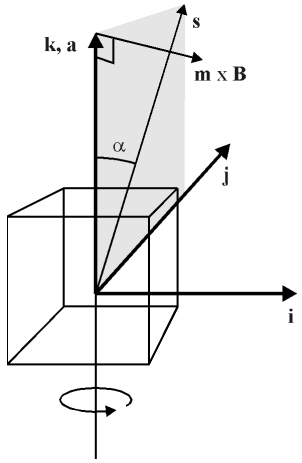

*Figure 2.9. The [**j**, **k**] plane (shaded) has a normal defined as **n** = **i** = **a** × **s**.*

where **a** is the spin axis (parallel to **k**), **B** is the Earth's magnetic field vector, **s** is the unit Sun vector and [**i**, **j**, **k**] are unit vectors in a coordinate system with the origin on the spin axis. The [**j**, **k**] plane is by definition equal to the [**s**, **a**] plane, α is the angle between **s** and **a** and **m** is a unit vector parallel to the magnetic dipole moment vector of the electromagnet. For verification, the dynamics equations of the system will be derived, starting with the electromagnet which has a magnetic dipole moment **M** (unit vector **m**) parallel or antiparallel to the spin axis:

$$\mathbf{m} = u\mathbf{k} \tag{2.39}$$

Here u = { the polarity of the dipole moment of the electromagnet } = $\pm$ 1.

Introducing a unit vector **b**, parallel to the Earth's magnetic field and corresponding to the unit vectors **i**, **j**, **k**, it is possible to compute the torque

T (unit vector **t**) experienced by the electromagnet. With the scalar magnitude B of the Earth's magnetic field, the torque becomes:

$$\mathbf{T} = B\mathbf{m}\times\mathbf{b} = uB(0 \quad 0 \quad 1)\times(b_x \quad b_y \quad b_z) = uB(-b_y \quad b_x \quad 0) \tag{2.40}$$

Assuming that Victoria spins without nutation or other deviations from an ideal rotation, the angular momentum of the satellite can be written as **L** = *L***a**. Conservation of **L** (according to classical mechanics) dictates that

$$\frac{d\mathbf{L}}{dt} = L\frac{d\mathbf{a}}{dt} \equiv \mathbf{T} \tag{2.41}$$

since the scalar magnitude of the momentum *L* is not changed by the torque of the electromagnet (proof omitted here); only by its direction along **a**. The time derivative of the spin axis vector can be visualized as a vector originating from the top of **a** with the scalar magnitude *T*/*L*. In other words, *d***a**/*dt* is making **a** turn around an axis defined by **a** × *d***a**/*dt*. If this vector has a component that is parallel to the normal of the plane defined by **a** and **s** (normal **n** = **a** × **s**), the vector **a** tends to align with **s**, reducing α. The condition that **a** × *d***a**/*dt* and **a** × **s** should be as parallel as possible can be expressed by stating that they must not have any component that is antiparallel. This gives the following:

$$\left(\mathbf{a}\times\frac{d\mathbf{a}}{dt}\right)\cdot(\mathbf{a}\times\mathbf{s}) > 0 \tag{2.42}$$

in which

$$\mathbf{a}\times\mathbf{s} = (0 \quad 0 \quad 1)\times(0 \quad \sin\alpha \quad \cos\alpha) = (-\sin\alpha \quad 0 \quad 0) \tag{2.43}$$

$$\mathbf{a}\times\frac{d\mathbf{a}}{dt} = \mathbf{a}\times(\mathbf{T}/L) = (0 \quad 0 \quad 1)\times u(B/L)(-b_y \quad b_x \quad 0) = \\ = u(B/L)(-b_x \quad b_y \quad 0) \tag{2.44}$$

Inserting Eqns. (2.43) and (2.44) into Eq. (2.42) yields:

$$\left(\mathbf{a}\times\frac{d\mathbf{a}}{dt}\right)\cdot(\mathbf{a}\times\mathbf{s}) = (-\sin\alpha \quad 0 \quad 0)\cdot u(B/L)(-b_x \quad b_y \quad 0) = \\ = ub_x(B/L)\sin\alpha > 0 \tag{2.45}$$

Since $B > 0$, $L > 0$ and $\alpha > 0$ always are true, u and b_x have to be of equal sign for the above expression to hold. Thus, the algorithm is formulated:

> The sign of the Earth's magnetic field parallel to **i**, perpendicular to the [**j**, **k**] plane, is determined by the magnetometer. The direction of the current through the electromagnet should be such that its magnetic dipole moment along the spin axis **a** has the same sign as the component of the Earth's magnetic field along **i**. When the angle α becomes sufficiently small, the current is turned off until the spin axis once again starts to drift away from the Sun vector.

3 IMPLEMENTATION

3.1 SPACECRAFT SIMULATION

In an age of powerful and inexpensive computers it has become more efficient and economical to test an engineer's design in a computer simulation than on an actual spacecraft. Simulations and analyses of control systems for satellites can be done in Matlab using a collection of functions called the Spacecraft Control Toolbox (SCT). Spacecraft control is often equivalent to attitude control, and considering the task at hand; to analyze a Sun-pointing control algorithm, it seemed appropriate to perform the simulations using this toolbox. The SCT, developed by Princeton Satellite Systems, is a vast collection of Matlab functions intended for attitude and orbit control of a spacecraft. Some of the functions that have been used are routines for computing and plotting orbital data (position and velocity of the satellite), CAD-functions (computes disturbances, see below), and two models of the Earth's magnetic field. Spacecraft simulation as well as any other type of simulation often involves modeling the dynamics of a system, which requires the equations of motion to be defined. In the case of attitude determination, the equations for rigid body rotation (Euler's equations) were used. Furthermore, the satellite is using the Earth's magnetic field in combination with a current through the coil to generate the desired torque. The current is controlled by the algorithm in conjunction with a Sun-sensor and a magnetometer. Functions for determining the Sun-vector as well as the magnetic field in spacecraft coordinates are available in the Spacecraft Control Toolbox.

3.1.1 Spacecraft CAD – Designing a Virtual Satellite

Within the Spacecraft Control Toolbox, several methods of building and simulating the flight of spacecraft are available. One method uses a rigid body assumption and treats the vessel as a point mass with a constant inertia matrix located at the CG to compute the attitude and the rates of rotation. This is the method used for the main attitude control simulations since it produces sufficient accuracy and is easy to code. However, there is one other method available in SCT that was used initially, to compute the magnitudes of the disturbance torques (see Section (2.4)) in order to determine whether these torques should be included in the attitude simulations or not. To compute disturbance forces, a more complex model of the spacecraft than the point mass model was required. By defining each major component of the satellite (core, solar arrays, antennae etc.) in a set of matlab functions collected under the name Spacecraft CAD, spatial calculations such as gravity gradient and temperature imbalances could be performed. The model of Victoria could then be launched into orbit and viewed in 'real-time' (computations were done in real-time, but the actual movement was slowed down significantly by the system) as it spun about its *z*-axis and followed the orbit path. A flowchart of the fundamental structure of a Spacecraft CAD model is displayed below as Fig. (3.1):

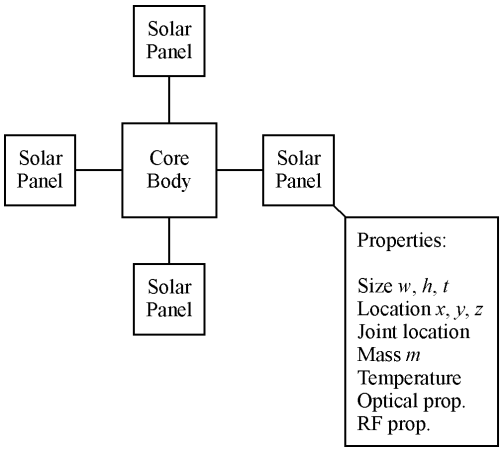

Figure 3.1. In order to calculate disturbances, many material parameters must be fed to the program.

where the size is defined by three values (width, height and thickness for a box), the location in 3D space is given by three cartesian coordinates *x*, *y*, *z* and the location of the joint to the previous compontent (the core body) also is written in cartesian coordinates. Furthermore, the mass *m* and the temperature, optical and RF properties of each component need to be determined in the form of material specific data.

The results from the CAD model computations showed that all the disturbance torques were *at least* one magnitude smaller than the torque induced by the electromagnetic coil, and can therefore be excluded from the attitude control simulations without altering the results noticeably.

3.1.2 Julian Day Numbers

When carrying out computations on astronomical properties such as orbit periods and planetary movement, it is convenient to use a system of numbering days based on integers instead of years, months and days. This system is called *Julian day numbers* and it facilitates determining the number of days between two dates (simply subtract one Julian day number from the other). The Julian day number system is sometimes said to have been invented by Joseph Justus Scaliger (1540 – 1609), one of the founders of the science of chronology. However, Scaliger's invention was not the system of Julian days, but rather the so-called Julian period. To arrive at this Julian period, Scaliger combined three traditionally recognized time cycles of 28, 19 and 15 years, obtaining a cycle of 7980 years (the least common multiple of 28, 19 and 15). The explanation in Encyclopedia Brittanica reads:

> *"The length of 7980 years was chosen as the product of 28 times 19 times 15; these, respectively, are the numbers of years in the so-called solar cycle of the Julian calendar in which dates recur on the same days of the week; the lunar or Metonic cycle, after which the phases of the Moon recur on a particular day in the solar year, or year of the seasons; and the cycle of indiction, originally a schedule of periodic taxes or government requisitions in ancient Rome."*

The first Julian period began with Year 1 on -4712-01-01 and will end 7980 years later on 3267-12-31, as a result of Christ's birth which was characterized by the number 9 of the solar cycle, the first Metonic cycle, and by number 3 of the indiction cycle (9, 1, 3). Scaliger chose as his initial epoch the year defined by (1, 1, 1), making the first year 4713 B.C. (Note that 4713 B.C. is the year -4712 according to the astronomical year numbering). For astronomers a Julian day begins at noon and runs runs until noon the following day. Decimals can be introduced to represent hours, minutes and seconds, for example: the Julian day number of 1996-03-31 at midnight is written 2450174.5. Conversions from Gregorian dates (used in daily life) to Julian day numbers are performed by a basic algorithm, where the Gregorian day, month and year are represented by (d, m, y):

$$jd = \left(1461 \cdot \left(y + 4800 + \left(m - 14\right)/12\right)\right)/4 + 367 - \left(3 \cdot \left(\left(y + 4900 + \left(m - 14\right)/12\right)/100\right)\right)/4 + d - 32075 \quad (3.1)$$

Here, days are integer values in the range 1-31, months are integers in the range 1-12, and years are positive or negative integers. The result of each division is truncated (remainders are discarded) as in integer arithmetic. The reversed conversion process (Julian day number to Gregorian date) can be carried out by employing another algorithm which is omitted here (shown in [9]). Julian date numbers are used in the advanced magnetic field model since the actual Earth magnetic field varies with time.

3.1.3 Orbit Environment Simulation

The Spacecraft Control Toolbox provides functions that simulate the orbit of a satellite by returning the position and velocity vectors at corresponding times. The input parameters to the function used are defined in a vector containing the Kepler elements as well as a time vector, defining the total number of computational points in the simulation. This function is based on the two-body problem and a spherically perfect Earth, resulting in a perturbation free orbit environment. Hence, the state vector of the satellite is calculated with Kepler's laws using the Kepler elements. The function also returns a plot of the satellite track around the Earth, see Fig. (3.2). The described model is acceptable for an attitude control simulation since long term effects on the orbit will not change the performance of the algorithm. However, functions for more accurate orbit calculations are also available in SCT, considering the orbit deviations due to the perturbing forces.

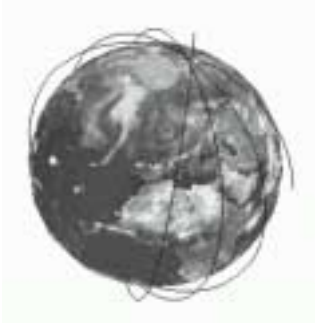

Figure 3.2. A 3D Satellite Track

A magnetic torquer depends on the Earth's magnetic field vector, making it necessary to model the geomagnetic field. Primarily, this was done with a simple dipole using the satellite position vector as the input parameter. Such a model is sufficiently accurate for a low altitude orbit such as Victoria's, but for higher altitude orbits or computations that require a higher degree of accuracy, a more detailed model may be used (see Section (3.3.1)).

The dipole function returns a magnetic field vector in the ECI frame. Simulation computations require a transformation of the magnetic field vector from the ECI frame into the body-fixed frame, an option that is provided in the SCT using either Euler or quaternion transformations (see Appendix A & B). Finally, the initial attitude of the satellite is specified

using Euler angles, which in turn are transformed into quaternions. The reason for this is that quaternions are numerically more efficient to use when propagating the attitude of the satellite using Runge-Kutta methods.

3.1.4 Solving the Euler Equations with the 4th Order Runge-Kutta Method

The attitude control simulations were all built around the same core loop, in which a numerical method was used to solve the previously derived Euler equations of motion (Eq. (2.33)), propagating the angular rate vector and the rotation quaternions (described in detail in Appendix B) for each time step. To achieve a sufficiently high degree of accuracy in the computations, the classical fourth-order Runge-Kutta method was employed, solving primarily for the ω_x, ω_y and ω_z components. The discretization error of this method is $O(h^4)$, where h is the time step used in the solution, meaning that the error $\varepsilon \rightarrow 0$ rather rapidly as h decreases in size. To illustrate the marked improvement brought about by increasing the order of a Runge-Kutta method from second to fourth, Fig. (3.3) has been added, showing two approximations to the function $f(t) = e^{-t}$:

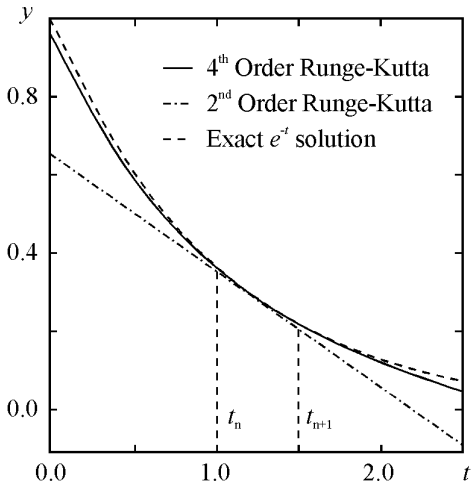

Figure 3.3. Different order solutions to e^{-t} (linear and cubic)

The fourth-order Runge-Kutta numerical integration method calculates the values of rotations and rates for the next time step using the following algorithm:

$$\mathbf{x}_{t+1} = \mathbf{x}_t + \frac{h}{6}\left(\mathbf{k}_1 + 2\left(\mathbf{k}_2 + \mathbf{k}_3\right) + \mathbf{k}_4\right) \tag{3.2}$$

where, for the problem at hand, **x** is the state vector on the form:

$$\mathbf{x} = \begin{bmatrix} q_1 & q_2 & q_3 & q_4 & \omega_x & \omega_y & \omega_z \end{bmatrix}^T \tag{3.3}$$

(the q:s being quaternion components). The parameters $\mathbf{k}_1$ through $\mathbf{k}_4$ of Eq. (3.2) are computed in the following way:

$$\begin{aligned}\mathbf{k}_1 &= f(\mathbf{x}, t)\\ \mathbf{k}_2 &= f\left(\mathbf{x}+\frac{h}{2}\mathbf{k}_1, t+\frac{h}{2}\right)\\ \mathbf{k}_3 &= f\left(\mathbf{x}+\frac{h}{2}\mathbf{k}_2, t+\frac{h}{2}\right)\\ \mathbf{k}_4 &= f(\mathbf{x}+h\mathbf{k}_3, t+h)\end{aligned} \tag{3.4}$$

where f is the right-hand-side of the differential equations and t is the current time. Numerical instabilities are easily introduced in the solving of differential equations, leading to divergence from the correct solution. Sources of such instabilities as well as suitable preventive actions are discussed further in Section (3.4.1) below.

3.1.5 Spacecraft Properties

Since the Victoria satellite is still under development as this report is being written, detailed models of the inertia matrix or component weights are not available. Instead, the inertia matrix was approximated using the definition of moments of inertia along with Steiner's theorem on a set of homogeneous boxes with different masses. The types of boxes used were:

Component name	Mass [kg]	Size [m]
Core Box	17	0.20 x 0.20 x 0.20
Solar Panel	1.2	0.20 x 0.20 x 0.01

Table 3.1. Five solar panels were used in the calculation of the inertia matrix.

After verification, the inertial products were found to be one magnitude less than the three moments of inertia I_{xx}, I_{yy}, I_{zz}. They were therefore set to zero to facilitate and speed up computations, which yielded the following inertia matrix:

$$\mathbf{I} = \begin{bmatrix} 0.2738 & 0 & 0 \\ 0 & 0.2738 & 0 \\ 0 & 0 & 0.3453 \end{bmatrix} \tag{3.5}$$

where the inertial moments have the unit [kgm^2]. The center of gravity for this model is located at 0.0274 m below the center of the core body and the total mass measures approximately 23 kg.

3.2 GRAHN'S ALGORITHM IMPLEMENTED

The Sun-pointing attitude control algorithm described in Section (2.5) will ultimately be written in computer code and fed into the payload computer, using the electromagnetic coil as its actuator. For simulation purposes, a Matlab function that performs the comparison between the Earth's magnetic field and the body fixed frame and then decides upon a suitable polarity of the coil current was created. This function is called once for each time step in the main simulation loop, giving the magnetic dipole moment that results

in a torque. A minimum angle α_{min} (between the spin axis of Victoria and the Sun vector) is also sent into the function, below which the coil current is cut off by giving it polarity 0 (instead of ±1). As soon as the satellite drifts off position, the coil is turned back on to correct the attitude. Below, a flowchart demonstrating the steps carried out in the function is shown:

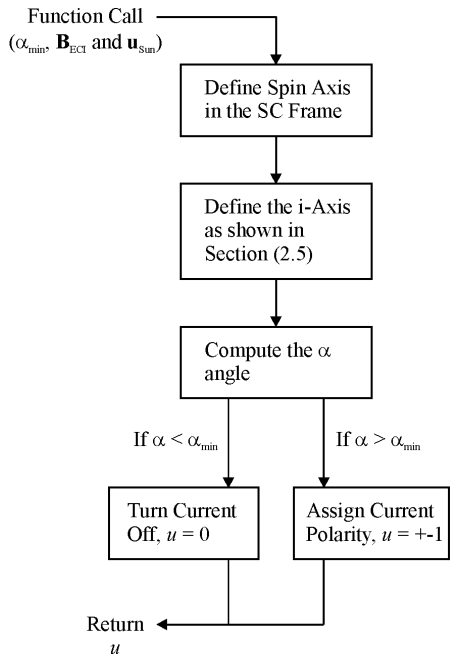

Figure 3.4. The main steps of the function `Grahn.m`

where $\mathbf{B}_{ECI}$ is the Earth's magnetic field vector in the ECI frame and $\mathbf{u}_{Sun}$ is the Sun vector in the spacecraft frame.

There are a few distinct discrepancies between the simulation code described above and the actual satellite control implementation. The first difference lies in the way signals from the magnetometer and Sun sensor are sampled; in the simulation they are sampled once for each time step, i.e. every ~ 0.1 seconds, while the satellite only samples a few times per minute. This means that the magnetic field vector and the Sun vector in the orbiting Victoria need to be recalculated in the payload computer, using the previous orientation and rates of rotation. However, errors introduced due to numerical computations in the satellite should not reach sufficiently high values to interfere with attitude control.

The second difference involves assumptions made about the Sun sensor in the simulation. In the code, the FOV of the sensor is assumed to be an ideal 180 degrees, while it in actuality is limited to 40° (or ± 20°). If a narrow FOV Sun sensor is used in Victoria it becomes crucial to initiate the spin rate at just the right time (with an angle $\alpha < 40°$ between the spin axis and the Sun vector) to avoid 'lost in space'-scenarios where the satellite cannot find the Sun.

3.3 SIMPLIFIED SIMULATION

To verify the main program and its functions, a series of somewhat simplified simulations were run in which the Earth's magnetic field was

approximated by a dipole (the specifics are discussed in Section (3.3.1)). Below, a flowchart of the Matlab simulation code, describing its contents step by step, is show as Fig. (3.5):

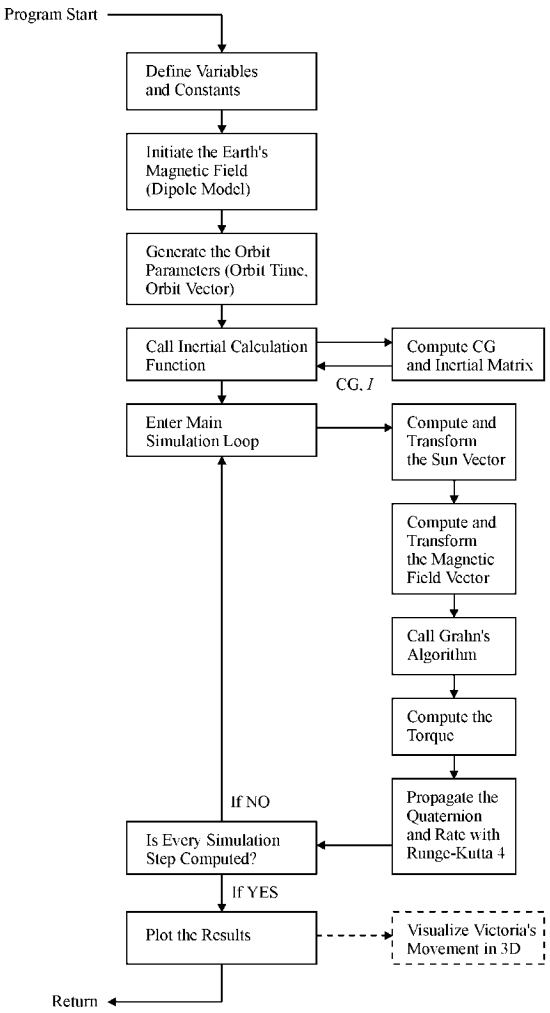

Figure 3.5. Flowchart of the simulation code

The majority of the steps have been described in previous sections, with one exception: 'Visualize Victoria's Movement in 3D', which executes a real-time visualization of the satellite's rotations, based upon the saved quaternions from each time step.

In the present configuration and with the inertia matrix of Eq. (3.5), the simulation failes to produce a converged solution with a decreasing α angle, regardless of the time step size. The result obtained for α can be viewed in Fig. (3.6) as a function of the simulation time. However, the problem of divergence can be solved, giving the desired attitude control behaviour, as is shown in Section (3.3.2).

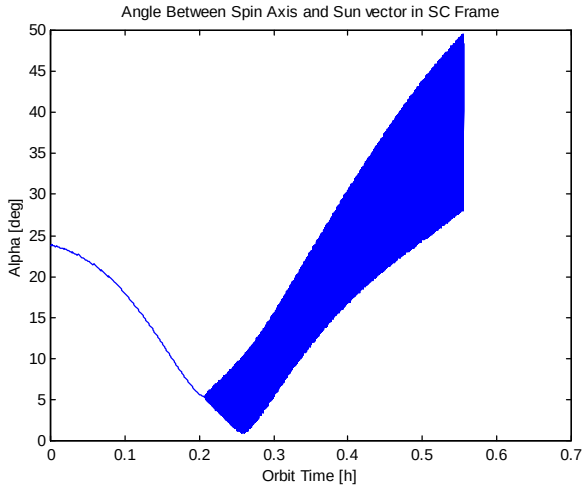

Figure 3.6. The angle between the spin axis and the Sun vector does not converge.

3.3.1 Approximation of the Magnetic Field

The Earth is essentially a gigantic magnet with poles called the North and South magnetic poles. These poles are located near the geographic North and South poles, respectively. The North magnetic pole attracts the north pole of a compass needle, so it is actually the south pole of the Earth magnet. Similarly, the South magnetic pole is the north pole of the Earth magnet since it repels the north pole of a compass needle. The magnetic field at the surface of the Earth, known as the geomagnetic field, varies in strength from 0.3 gauss to 0.6 gauss (the unit of magnetic induction or magnetic flux density, 10 000 gauss equals one tesla). As a comparison of magnitudes; the field near the poles of a small horseshoe magnet may be several hundred gauss and the fields of magnets used in industrial applications may measure more than 20 000 gauss (2 tesla).

It is the Earth's inner structure that creates the mentioned geomagnetic field. The crust of the Earth is the outermost portion on which we live and beneath it lies a rocky mantle. Under the mantle is a dense core, which has a solid inner part and a liquid outer part. Scientists believe that the motion of electric charges in the liquid outer core produces the geomagnetic field. The Earth's magnetic field also extends into space beyond the atmosphere, where it is called the magnetosphere. The magnetosphere interacts with a flow of charged particles from the Sun called the solar wind (see Section (2.4.1)). This interaction is the cause of different phenomena such as auroras and a zone of charged particles around the Earth known as the Van Allen-belts. Furthermore, the impact of the solar wind causes the magnetic field lines facing sunward to compress, while the lines facing away from the Sun stream back to form the Earth's so-called magnetotail. Hence, the magnetosphere is shaped like a teardrop, with the point extending away from the Sun, see Fig. (2.7). The magnetosphere extends into the vacuum of space from approximately 80 to 60 000 kilometers on the side towards the Sun, and trails out more than 300 000 kilometers away from the Sun.

In its most basic magnetic form, Earth can be thought of as a dipole magnet (bar magnet). The "best fit" of this dipole to the observed magnetic

field is obtained by placing a dipole of magnetic moment $8 \cdot 10^{22}$ Am^2 about 400 km from the center of the Earth, with the axis of the dipole at an angle of 11.5° relative to the Earth's axis of rotation. Although this magnetic field is symmetrical unlike the magnetic field of Earth, it provides a reasonably accurate approximation. This can be motivated by the fact that Victoria will be orbiting at the relatively low altitude of 700 km above sea level, where the actual field is fairly symmetrical. Also, the strength of the nondipolar field (the difference between the actual field and the "best fit" dipole field) is, on average, only about 5% of the total field (although there can be much greater local anomalies).

The attitude control algorithm was tested using the simple dipole model and proved to be stable for many different initial values of the attitude, as will be shown further ahead. In Section (3.4), simulations are run using functions provided by SCT for more accurate modeling of the magnetic field (see Fig. (3.7)), where actual measurements of the Earth's magnetic field are read from a data file based on the IGRF model described in [10].

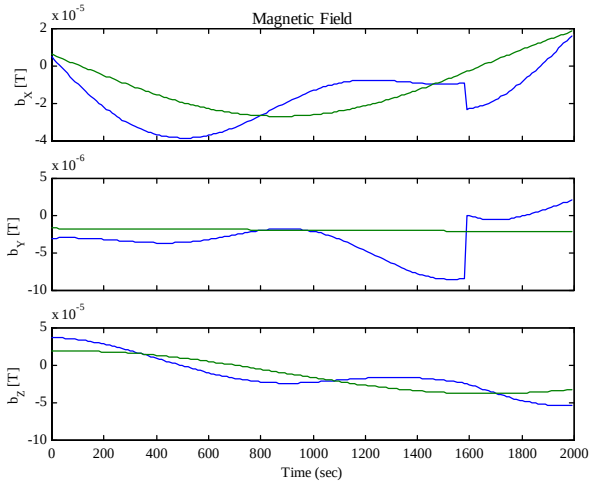

Figure 3.7. The oscillating lines with the singularities represent the advanced IGRF magnetic field model, while the other ones show magnitudes of the dipole approximation components.

3.3.2 Inertia Matrix Adjustments

In this first paragraph, a few facts about the inertia matrix are recapitulated to facilitate understanding of the second paragraph, where the adjustments are described. It can be shown that there is one unique orientation of axes *x-y-z* for a given origin for which the products of inertia vanish and the moments of inertia I_{xx}, I_{yy} and I_{zz} assume stationary values. For this orientation, the inertia matrix (or inertia tensor) takes on the form of Eq. (3.5). This diagonal matrix contains the principal moments of inertia, which were calculated by treating the sections (core body + five sun panels) of the satellite as boxes or *rectangular paralleleppipedes*. That model is a good approximation for the inertia tensor if the satellite has an even (homogeneous) mass distribution. The actual inertia tensor is difficult to predict and should therefore be measured on the actual satellite in a lab environment. Such tests have not been carried out (as this report is being written), which motivates an even-mass-distribution approximation of the satellite. For a spinning satellite to be stable, the mass distribution needs to

resemble that of a disc (with the spin axis in the same direction as the normal of the disc). This is an important consideration when constructing a spin-stabilized satellite.

In the case where the satellite is symmetrical around the spin axis ($I_{xx} = I_{yy}$), the *moment of inertia ratio* λ should be greater than 1.1, where $\lambda = I_{zz}/I_{xx}$. The inertia matrix of Eq. (3.5) is more similar to a sphere than to a disc, making the satellite somewhat unstable. However, note that the stability parameter for a spin-stabilized satellite is satisfied in this matrix ($\lambda = I_{zz}/I_{xx} > 1.1$). Nevertheless, the moment of inertia ratio λ was increased by reducing the magnitudes of I_{xx} and I_{yy} to half their initial magnitudes, while at the same time I_{zz} was increased with a factor of two. Increasing λ by a factor of four proved to be sufficient to stabilize the satellite, as can be seen in Figs. (3.9) – (3.12). Physically, this can be achieved by positioning weights at the outer edges of the solar panels (see Fig. (3.8)) or reducing the height of the core box considerably. The adjusted inertia matrix yields the benign attitude behaviour presented in Figs. (3.9) & (3.10):

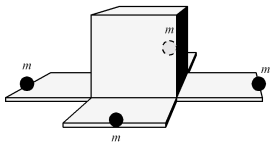

Figure 3.8. Point masses can increase the oblateness.

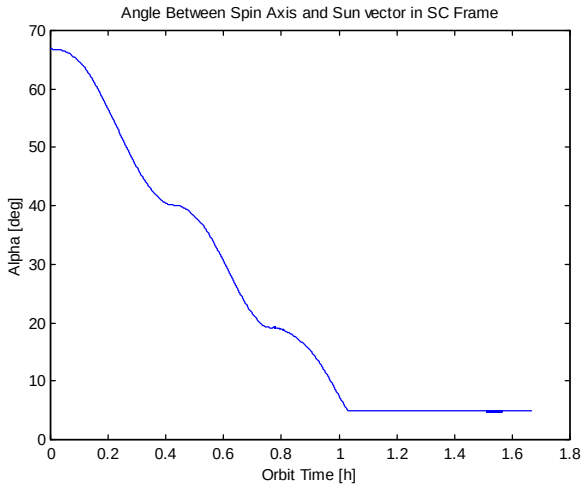

Figure 3.9. Starting with an α of ~ 67°, Victoria succesfully aligns within $\alpha_{min} = 5°$ of the Sun vector.

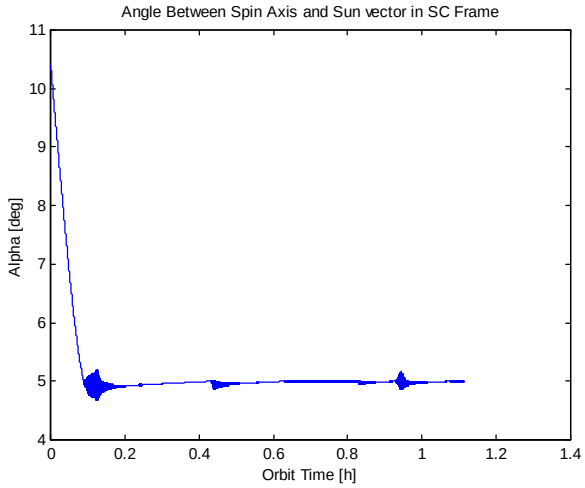

Figure 3.10. The satellite maintains its attitude at $\alpha \approx 5°$.

3.4 REALISTIC SIMULATION

In order to further increase the accuracy of the dynamic behaviour of Victoria during attitude control, a somewhat more complex simulation than the one presented in Section (3.3) was executed. It incorporated the use of the realistic magnetic field model demonstrated in Fig. (3.7), in which the field vector has a slightly larger magnitude than the vector in the dipole approximation. If the magnitude of the current remains unchanged compared to the previous simulations, this yields a stronger torque on the satellite. The resulting solutions showed a tendency to diverge in a fashion similar to Fig. (3.6) above, but could be made to converge under certain conditions: Most importantly, the inertia matrix adjustments made under Section (3.3.2) were required in the realistic simulation as well. Furthermore, a weaker current could be used to slow down the attitude change of the satellite and thereby avoid divergence (this was not required in the simulations shown below in Figs. (3.11) & (3.12)).

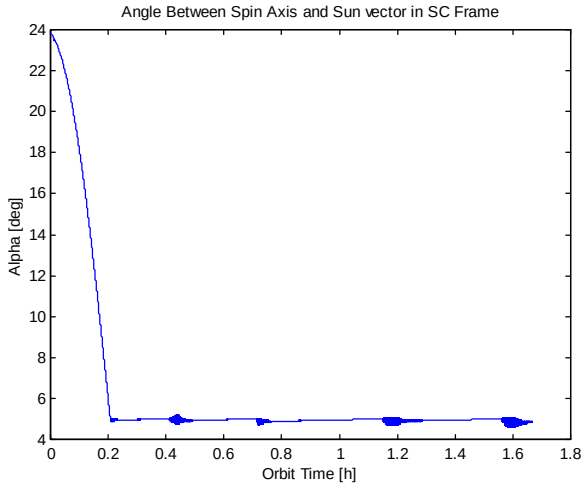

Figure 3.11. Victoria aligns with the Sun vector from an initial 24° α angle.

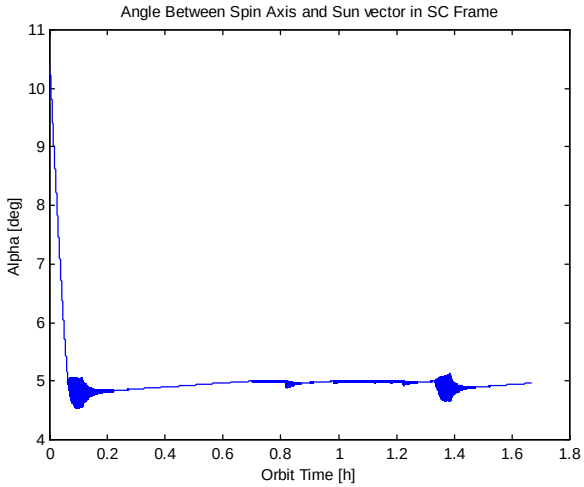

Figure 3.12. Even with the oscillative magnetic field model, the satellite manages to hold its attitude.

3.4.1 Sources of Instabilities

The Runge-Kutta propagation of the satellite's attitude quaternions relies on numerical methods to compute the dynamics for the next time step. This numerical solution to the governing differential equations depends on parameters fed to the computer in the form of time step size *h*, coil current, spin rate and magnetic field vector. For a computation based on an equal time step size (i.e. *h* is constant), an upper bound for the error introduced by the numerical method can be calculated using the so-called *Composite Simpson's rule* which is given by:

$$E_{CS} \leq \frac{M_4}{2880}(b-a)h^4 \tag{3.6}$$

where M_4 is a bound for the fourth derivative of the equation used and $b - a$ is the length of the interval for the current time step. Employing Simpson's rule, the numerical error could be kept arbitrarily small as long as the fourth derivative M_4 is known. However, for the application at hand, a simpler method for veryfying the accuracy of the numerical results can be used: By running the the same simulation several times in a row and only changing the time step *h*, the convergence of the obtained solutions can be tested. If the computations vary sufficiently little, a suitable *h* has been found.

Other sources that can cause divergence in the computations are the coil current and the magnetic field vector magnitude. If either one of these becomes too large, the torque affecting the satellite reaches values that attempt to rotate it at a higher rate, equivalent to increasing the interval $b - a$ above, and thereby increasing the error. Thus, a slower settling behaviour is more accurately computed than a rapid one.

3.5 POWER CONSUMPTION

While adjusting the attitude of Victoria, the electromagnetic coil consumes a certain amount of power in the form of supplied current. This power consumption can be calculated for different scenarios (starting at angles α of 67°, 24° or as low as 5°) and different time periods. The time periods can be chosen as one orbit, one average orbit, one hour or the time needed to reach a desired α.

The power calculations are primarily used to verify that the total average orbit power of the satellite (16-20 W) is not exceeded. Furthermore, comparisons of the effectiveness of different actuators (3 coils, 1 coil, reaction wheels) are facilitated, which can help determine the most suitable means of control. The equation governing consumption of power *P* in any electrical device is given by:

$$P = IU \tag{3.7}$$

where *I* is the current in amperes and *U* is the voltage. If the electrons in the current are moving through a resistive medium, such as a conductor, the relation $U = IR$ gives the following:

$$P = I^2 R = \frac{U^2}{R} \tag{3.8}$$

with R being the resistance in ohms. The SI-unit for power is the watt (W), and power during a time period is usually measured in wattseconds (Ws) or watthours (Wh).

For power efficiency comparisons, a number of simulations have been carried out, starting at three different α angles and using both magnetic field models. Computations of the power consumption were done under the assumption that the coil voltage measured approximately 10 V while engaged and the target α was set to 5°. As long as the satellite has not reached the 5° target angle, it is working with a constant power consumption of 10 Watts. As a result, an initial angle of 67° produces a settling time of approximately 1 hour, while for an angle of 24° the satellite takes roughly 15 min to settle (16 min for the dipole model and 12 min for the realistic model). The results are presented in the following table:

	Power Consumption [W]	
Initial α Angle	Dipole Magnetic Field	Realistic Magnetic Field
>5°	10	10
~5°	1 (average)	0.6 (average)

Table 3.2. Power consumptions for different initial attitude scenarios

where the average power is computed by dividing the total energy consumption (Ws) by the simulation time (s).

It is apparent that the realistic magnetic field model produces a higher field strength, leading to a greater torque. It therefore requires less power to control the attitude.

4 CONCLUSIONS

The most fundamental conclusion that can be drawn from our simulations is that the Sun-pointing algorithm by Sven Grahn successfully aligns the spin axis of Victoria with the direction to the Sun. One of the strong points of this algorithm is its simplicity in implementation, requirering only a few mathematical operations in the payload computer at each time step. Another strength is the ability to accomplish with one coil what usually is done with two or three coils - namely controlling the attitude of Victoria in a stable manner. Furthermore, the satellite is for an arbitrary angle α able to reach that angle in a short amount of time and maintain that attitude without diverging.

The importance of an oblate mass configuration, i.e. a shape that closer resembles a disc than a sphere, became apparent during the simulations as the satellite showed tendencies to be unstable. However, by redistributing Victoria's mass and thereby modifying the inertia matrix, stability could be achieved. Other factors to consider in order to obtain a stable behavior in the simulations were the time step size in the Runge-Kutta method, the dipole moment of the actuator coil (governed by the magnitude of the current), the spin rate and the magnitude of the magnetic field vector.

The disturbance forces acting on the satellite all measured at least one magnitude less than the attitude control torque, a fact that was verified using the Spacecraft CAD functions in the SCT. Long term effects of these minute disturbance forces need not be considered for this basic application as the control algorithm counteracts any deviation from the assigned α, regardless of its origin.

Choosing the current magnitude was done by investigating the magnetic dipole moment generated by actuators of similar satellites. This resulted in a first assumption for the coil current of 1 Ampere, that with a voltage of 10 V in the coil yielded the maximum 10 Watt power consumption. Combined with the realistic magnetic field model, the time for Victoria to settle at α = 5° from an initial angle of 67° then became approximately 1 hour.

Average orbit power differs between the two magnetic field models due to the mentioned discrepancy in field strength magnitude. Simulations with the IGRF model consumes 60% of the power used with the dipole approximation. Another factor determining the power consumed to maintain a desired attitude is the inertia matrix components (smaller moments of inertia results in increased mobility but also raises susceptibility to disturbances). Note that the computed power usage of 0.6 W is based on a number of approximations, but nevertheless provides a reasonable basis for comparisons with other control methods.

ACKNOWLEDGEMENTS

We would like to thank Thomas Lindblad and Hanno Essén at KTH for guidance and support throughout the course of the project. We would also like to thank Sven Grahn at SSC for helping us with the algorithm and Ola Widell for inspiration and motivation during our visit at the Esrange launch site. Furthermore, we are grateful toward Olle Norberg at IRF for being kind enough to comment on our report while we were at lunch, as well as other members at IRF for making our stay in Kiruna a pleasant one. The work presented in this report has been financed by the Knut and Alice Wallenberg Foundation. Finally, Mike Paluszek at Princeton Satellite Systems helped us with questions regarding the SCT, which was greatly appreciated.

REFERENCES

[1] The Munin satellite site,
http://munin.irf.se/

[2] The Hugin satellite site,
http://www.particle.kth.se/~fmi/hugin/huginstart.html/

[3] Jonsson & Kollberg, *Attitude Control of a Nanosatellite using Reinforcement Learning Neural Networks*, the Royal Institute of Technology (KTH), Stockholm, Sweden, October 1st (1999)

[4] Grahn Sven, *An On-board Algorithm for Automatic Sun-pointing of a Spinning Satellite*, Swedish Space Corporation, Sweden

[5] *Rymdsystem och Rymdteknik*, Institutionen för Materialens Processteknologi & Metallernas Gjutning, the Royal Institute of Technology (KTH), Stockholm, Sweden, (1999)

[6] Chobotov Vladimir A., *Orbital Mechanics - 2nd Ed.*, AIAA Education Series, Virginia, (1996)

[7] Spiegel Murray R., *Theoretical Mechanics (Metric Ed.)*, McGraw-Hill Book Company, (1982)

[8] Benson Harris, *University Physics (Revised Ed.)*, John Wiley & Sons, (1996)

[9] http://serendipity.magnet.ch/hermetic/cal_stud/jdn.htm

[10] An IGRF magnetic model site,
http://www.ngdc.noaa.gov/IAGA/wg8/igrf2000.html

[11] Shoemake Ken, *Animating Rotation with Quaternion Curves*,
Computer Graphics V.19 N.3, (1985)

APPENDIX A – EULER ANGLES

It is convenient to specify the motion of a rigid body relative to a set of coordinate axes coinciding with the principal axes which are fixed in the body and consequently rotate as the body rotates. The orientation of the satellite is given by a series of three consecutive rotations, *the Euler angles*, whose order are important (there are several conventions governing the order and orientation of the rotations, for instance *z-x-z′* or *z-y-x*). These rotations are relative to the inertial *space axes*, which are fixed in space. The satellite is initially imagined to be oriented so that its axes are parallel to those fixed in space. The following rotations are then applied (see Fig. (A.1)):

1. A rotation ϕ about the *z*-axis of both the inertial and body frame.
2. A rotation θ about the new *x*-axis (at *A*) of the body frame.
3. A rotation ψ about the *z′*-axis of the body frame.

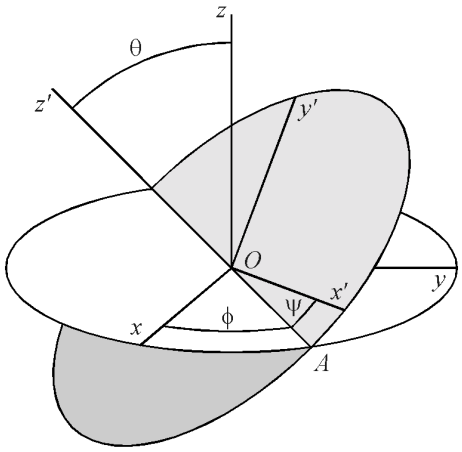

Figure A.1. The line OA is referred to as the Line of Nodes (see Fig. (2.2)).

This makes it possible to transform a vector in the ECI (Earth-Centered Inertial) coordinates into body fixed coordinates (satellite coordinates). For example, consider the magnetic field vector $\mathbf{B}_{\mathrm{ECI}}$ defined in the space axes. This vector can be represented in body fixed coordinates $\mathbf{B}_{\mathrm{BF}}$ through a series of transformation matrices. These matrices shown below:

$$\mathbf{L}_1(\phi)=\begin{bmatrix}\cos\phi & -\sin\phi & 0\\ \sin\phi & \cos\phi & 0\\ 0 & 0 & 1\end{bmatrix} \tag{A.1}$$

$$\mathbf{L}_2(\theta)=\begin{bmatrix}1 & 0 & 0\\ 0 & \cos\theta & -\sin\theta\\ 0 & \sin\theta & \cos\theta\end{bmatrix} \tag{A.2}$$

$$\mathbf{L}_3(\psi)=\begin{bmatrix}\cos\psi & -\sin\psi & 0\\ \sin\psi & \cos\psi & 0\\ 0 & 0 & 1\end{bmatrix} \tag{A.3}$$

which yields the following transformation from the ECI frame to the body fixed frame:

$$\mathbf{B}_{BF}=\mathbf{L}_3(\psi)\cdot\mathbf{L}_2(\theta)\cdot\mathbf{L}_1(\phi)\cdot\mathbf{B}_{\mathrm{ECI}} \tag{A.4}$$

where the order of the matrices is crucial. However, some sequences of rotations will result in the same orientation. For example, considering a book laying on a table face up, define the *x*-axis to the right, *y*-axis up, and the *z*-axis normal to the tabletop. A rotation of π radians about the *y*-axis will turn the book so that the back cover is now facing up. Another way to achieve the same orientation would be to rotate the book π radians about the *x*-axis, and then π radians about the *z*-axis. To avoid ambiguities, the Euler angle*s* are limited to:

$$-\pi \le \phi < \pi \quad \text{or} \quad 0 \le \phi \le 2\pi$$

$$-\pi / 2 \le \theta \le \pi / 2$$

$$-\pi \le \psi < \pi \quad \text{or} \quad 0 \le \psi \le 2\pi$$

The angles will then be unique for most orientations of the satellite, but for a continuous steady rotation, around one of the principal axes, the time variation of one of the angles is a discontinuous sawtooth function. This, along with other troublesome phenomena, can be avoided by using quaternions (see Appendix B) to define the orientation and rotation of the satellite. A quaternion is another way of representing the orientation of one frame with respect to another. Propagations of orientation are most efficiently done with quaternions and they are often used for numerical integration, due to the fact that quaternions have only 4 elements instead of the 9 transformation matrix elements. The Euler angles are still employed, since they give a physical picture of the satellite's attitude in contrast to the quaternions (which are impossible to visualize).

APPENDIX B – QUATERNION ROTATION

While it is possible to rotate objects in three dimensions using transformation matrices (as described in Appendix A), propagating rotations of a satellite governed by differential equations is easier done with quaternions. The basis of quaternion theory comes from complex numbers, where it is known that *i* represents the square root of –1, giving

$$i \cdot i = -1 \tag{B.1}$$

Any complex number can then be expressed in terms of real numbers, using a real and a complex part:

$$z = a + bi \tag{B.2}$$

Quaternions are an extension of complex numbers. Instead of just *i*, three different numbers *i, j, k* are introduced, all equal to the square root of –1:

$$\begin{aligned} i \cdot i &= -1 \\ j \cdot j &= -1 \\ k \cdot k &= -1 \end{aligned} \tag{B.3}$$

When multiplied together in pairs, these numbers behave similarly to cross products of the unit basis vectors.

$$\begin{aligned} i \cdot j &= -j \cdot i = k \\ j \cdot k &= -k \cdot j = i \\ k \cdot i &= -i \cdot k = j \end{aligned} \tag{B.4}$$

The conjugate and magnitude of a quaternion are calculated in practically the same way as complex conjugate and magnitude. For an arbitrary quaternion **q** they become:

$$\mathbf{q} = w + xi + yj + zk \tag{B.5}$$

$$\mathbf{q}' = w - xi - yj - zk \tag{B.6}$$

$$\|\mathbf{q}\| = \sqrt{\mathbf{q} \cdot \mathbf{q}'} = \sqrt{w^2 + x^2 + y^2 + z^2} \tag{B.7}$$

Quaternions are *associative* $(\mathbf{q}_1 \cdot \mathbf{q}_2) \cdot \mathbf{q}_3 = \mathbf{q}_1 \cdot (\mathbf{q}_2 \cdot \mathbf{q}_3)$ (B.8)

Quaternions are *not commutative* $\mathbf{q}_1 \cdot \mathbf{q}_2 \neq \mathbf{q}_2 \cdot \mathbf{q}_1$ (B.9)

The inverse of a unit quaternion (length 1) is equal to its conjugate, $\mathbf{q}^{-1} = \mathbf{q}'$.

A quaternion can be represented in a number of ways, of which three are shown here:

1. as a linear combination of 1, *i*, *j*, *k*,
2. as a vector of the four coefficients in this linear combination,

3. or as a scalar for the coefficient of 1 and a vector for the coefficients of the imaginary terms:

$$\begin{aligned} \mathbf{q} &= w + xi + yj + zk = \begin{bmatrix} x & y & z & w \end{bmatrix} = \begin{pmatrix} s, & \mathbf{v} \end{pmatrix} \\ s &= w \\ \mathbf{v} &= \begin{bmatrix} x & y & z \end{bmatrix} \end{aligned} \tag{B.10}$$

To compute rotations using quaternions, a unit vector **u** around which the rotation is performed will be needed, as well as an angle θ. By first constructing the quaternion **q** = (*s*, **v**), where

$$\begin{aligned} s &= \cos\frac{\theta}{2} \\ \mathbf{v} &= \mathbf{u}\sin\frac{\theta}{2} \end{aligned} \tag{B.11}$$

and then carrying out a standard matrix multiplication to rotate an arbitrary point **p** in space (employing the temporary quaternion **P** = (0, **p**)), the rotated point is obtained:

$$\mathbf{P}_{rotated} = \mathbf{qPq}^{-1} \tag{B.12}$$

Recalling that for a unit quaternion, the inverse is equal to the conjugate, the computation is simplified further. If several contributions $\mathbf{q}_1$, $\mathbf{q}_2$, … to a rotation need to be concatenated into one step the following method is used (similar to matrix transformation):

$$\mathbf{P}_{rotated} = \mathbf{q}_2\mathbf{q}_1\mathbf{P}\mathbf{q}_1^{-1}\mathbf{q}_2^{-1} \tag{B.13}$$

For further theory on the subject of quaternions, see [11].

APPENDIX C – MATLAB FUNCTIONS

Below, the matlab files written by the authors and employed in the simulations are listed along with a short description of their contents:

`Grahn.m`	The Sun-Pointing Algorithm by Sven Grahn implemented as described in Fig. (3.4).
`Victoria3D.m`	Animates the attitude change due to the applied torques by transforming an initial model of the satellite with the saved quaternions from the main simulation loop.
`VictoriaEnergy.m`	Computes the energy consumed by Victoria during the entire simulation as described in Section (3.5).
`VictoriaInert.m`	Delivers the inertia matrix along with the center of gravity for a Victoria model based on the dimensions and masses of the main components.
`VictoriaSim.m`	The main program, which defines constants and calls on each one of the functions described above. This code contains the core loop that performs the Runge-Kutta 4^{th} order propogation of the Euler equations and the quaternions.